Common-path interferometer for frequency-domain optical coherence tomography

Andrei B. Vakhtin, Daniel J. Kane, William R. Wood, and Kristen A. Peterson

A Michelson-type spectral interferometer that uses a common beam path for the reference and the sample arms is described. This optical arrangement is more compact and stable than the more commonly used dual-arm interferometer and is well suited for frequency-domain optical coherence tomography of biological samples. With a 16-bit CCD camera, the instrument has sufficient dynamic range and resolution for imaging to depths of 2 mm in scattering biological materials. Images obtained with this spectral interferometer are presented, including cross-sectional images in a *Xenopus laevis* tadpole.

OCIS codes: 120.3180, 170.3880, 170.4500.

1. Introduction

Low-coherence optical interferometry methods, such as optical coherence-domain reflectometry and spectral interferometry (SI), provide high resolution, subsurface depth profiling, and cross-sectional imaging with relatively simple optical arrangements and inexpensive light sources. These techniques are based on broadband or white-light interferometry, in which surface or depth profiling is obtained through the measurement of optical path-length or phase differences between the sample and the reference arms of an interferometer. When applied to two- or three-dimensional imaging for biological or medical applications, these techniques are referred to as optical coherence tomography (OCT).

OCT is typically executed in the time domain by use of a Michelson interferometer in which the optical path length of the reference arm is modulated. Phase modulation of the interferometer's reference arm is required to allow interference from reflective loci at different depths in the sample. Phase-sensitive detection of the interferometer output provides high dynamic range and depth-resolved measurement of light reflected or backscattered from the sample. Images are obtained when the light beam is scanned across the sample. High-speed image acquisition requires high-speed reference arm modulation, which cannot be done simply with the mechanical movement of a mirror. Other methods, such as piezoelectric fiber stretchers[1] and rapid-scanning phase-control delay lines,[2,3] have successfully allowed video-rate OCT imaging. However, these methods can be thermally or mechanically unstable. For medical applications in particular, it is desirable to minimize the number of moving parts in an instrument.

SI is used for frequency-domain implementation of low-coherence interferometry. A stationary interferometer is used, and the spectrally dispersed output of the interferometer (the spectral interferogram) is recorded. The signal returning from the sample arm can be thought of as a superposition of monochromatic waves that interfere with similar components in the reference arm. This interference leads to fringes on the spectrum. Depth information is encoded in the fringe frequencies and is easily obtained by Fourier transform of the spectral interferogram. Two-dimensional images can be obtained directly by use of line illumination and a camera,[4] whereas three-dimensional images can be obtained when the light beam is scanned across the sample. With SI, signals generated from all accessible sample depths are recorded simultaneously.

When one performs OCT, it important to compensate for dispersion and polarization differences between the two interferometer arms to avoid phase differences between the reference and the sample arms that are not due to the sample. One typically does this by having matched optical elements (lenses,

The authors are with Southwest Sciences, Inc., 1570 Pacheco Street, Suite E-11, Santa Fe, New Mexico 87505. K. A. Peterson's e-mail address is peterson@swsciences.com.

Received 17 December 2002; revised manuscript received 3 July 2003.

0003-6935/03/346953-06$15.00/0

filters, fibers, and associated polarization compensators) in each arm. Because SI uses a fixed interferometer, it is possible for the sample and reference arms to share the same beam path with the reference plane defined by an optical surface near the front surface of the sample. This arrangement provides automatic compensation for polarization and dispersion effects caused by optical elements in the interferometer. The common-path interferometer is easier to align; when the position of an optic in one arm is moved, there is no need to make a compensating adjustment in the other arm. The shared optical path also increases the interferometer's stability and reduces its sensitivity to vibrations because beam overlap is automatically maintained. The simplicity, stability, and compactness make this interferometer design attractive for medical applications. It is easily implemented with fiber optics, and the reference plane can be defined by any appropriate flat optical surface at the distal end of the fiber, including the fiber face.

The advantage of frequency-domain OCT or SI for biomedical imaging lies in the fact that the depth information is obtained in parallel. This eliminates the need for reference arm modulation, increasing the stability and simplicity of the instrument. Faster data-acquisition rates are inherent in the parallel data acquisition. However, the drawback is that it is a dc measurement method, which limits the dynamic range. Time-domain OCT, on the other hand, is an ac measurement method in which phase-sensitive detection at the reference arm modulation frequency allows shot-noise-limited detection and a high dynamic range of typically 100–110 dB. Dynamic range is particularly important in biological imaging, in which high scattering reduces signals exponentially with sample depth. Because of this, biomedical applications of SI have been limited outside the field of ophthalmology, in which scattering is low. One exception is the imaging of skin by Häusler and Lindner,[5] who used a linear photodiode array to record the spectral interferogram. They achieved a dynamic range of 79 dB but at the expense of long exposure times owing to the large area of the photodiodes.

Use of a silicon CCD camera for this application is desirable for its high sensitivity and two-dimensional detection area. As shown by Zuluaga and Richards-Kortum, using a two-dimensional camera and line illumination allows simultaneous detection of depth and one transverse direction.[4] This can greatly reduce the time needed to acquire a three-dimensional image. However, the 8-bit CCD camera used in that research can provide, at best, a dynamic range of 48 dB, which is insufficient for imaging in scattering media. We show that by using a high dynamic range, 16-bit CCD camera, SI can be successfully used for imaging in scattering biological tissues.

2. Principles of Spectral Interferometry

The principles of SI have been detailed in the literature.[6,7] A brief summary is given here to illustrate the procedure for obtaining depth information from a spectral interferogram. The optical apparatus for SI is quite similar to that used for time-domain OCT and is usually based on a Michelson interferometer. A spectrally broad, low-coherence beam is split into a *fixed* reference arm and a sample arm. Light reflected or scattered from the sample recombines and interferes with the reference beam. The interferometer output is sent through a spectrograph to resolve the interference fringes.

Depth information is encoded in the frequency of the fringes. A simple Fourier transform extracts the depth information. With SI, all depth information is acquired simultaneously, eliminating the need for reference arm modulation. The spectrum of the interferometer output is given by

$$I_{\mathrm{SI}}(\omega) = I_R(\omega) + I_S(\omega) + 2\sqrt{I_R(\omega)}\ \sqrt{I_S(\omega)} \times \cos[\phi_S(\omega) - \phi_R(\omega) - \omega\tau], \quad (1)$$

where $I_{\mathrm{SI}}(\omega)$ is the interferometer output spectrum, expressed as intensity as a function of optical frequency ω. $I_R(\omega)$ is the spectrum of the light in the reference arm, and $I_S(\omega)$ is the spectrum of the light returning from the sample arm. $\phi_R(\omega)$ is the reference arm phase, $\phi_S(\omega)$ is the sample arm phase, and τ is a fixed optical delay between the two arms chosen by the experimenter (see below).

Equation (1) consists of three terms. The first two terms are simply the reference and sample arm spectra. The third term is the interference between the reference and the sample arms and contains the depth (phase) information. This is a simplified presentation. Not shown are autocorrelation terms, which arise from interference between surfaces within the sample. Autocorrelation terms can appear as artifacts and coherent noise in SI images, reducing the image clarity and dynamic range.[5,8]

To facilitate extracting the depth-resolved signal from the SI output, we choose τ to yield fringes in the sum spectrum, i.e., so that the optical paths are nearly equal. This delay then remains fixed, and optical path differences resulting from backscattering or reflection from various depths in the sample are encoded in the interference fringes. The spectral fringes have a period inversely proportional to the optical path difference between the two beams.

Figure 1 shows the steps required to obtain the phase difference between the two arms. As an example, we will calculate the result for a single reflecting surface. Figure 1(a) shows the model spectrum of a spectrally broad input beam. Figure 1(b) shows the output spectrum, $I_{\mathrm{SI}}(\omega)$. The fringe spacing is proportional to the optical delay between the two arms. The first step is to subtract the individual spectra, $I_R(\omega)$ and $I_S(\omega)$, to isolate the spectral interferogram $S(\omega)$, where

$$S(\omega) = 2\sqrt{I_R(\omega)}\ \sqrt{I_S(\omega)}\cos[\phi_S(\omega) - \phi_R(\omega) - \omega\tau]. \quad (2)$$

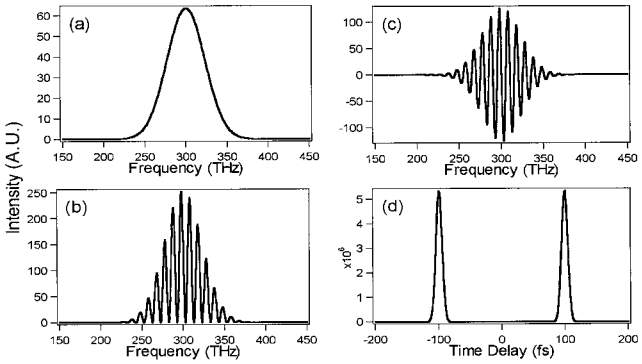

Fig. 1. Calculated SI data for a single reflective surface. (a) Input light-source spectrum. (b) Output spectral interferogram. (c) Spectral interferogram with the input spectrum removed. (d) Fourier transform of the spectral interferogram.

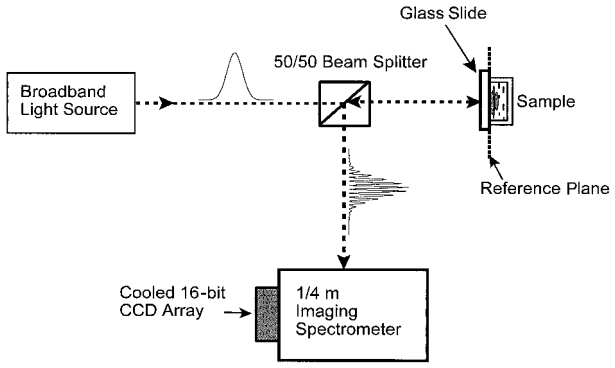

Fig. 2. Schematic of the SI in which the reference and sample arms share the same beam path. The reference plane is defined by the back surface of the glass plate. Lenses are excluded from the schematic for clarity. See text for details.

The result is shown in Fig. 1(c). By Fourier transforming $S(\omega)$, we obtain

$$\mathcal{F}^{-1}[S(\omega)] = f(t - \tau) + f(-t - \tau), \tag{3}$$

where $f(t)$ is the correlation product between the reference and the sample fields [Fig. 1(d)]. In this example, reflection from a single depth in the sample results in a simple function of intensity-versus-time delay. Note that mirror images of $f(t)$ occur at positive and negative delays. The time delay corresponds directly to distance.

$I_S(\omega) \simeq I_R(\omega)$ when there is no significant absorption by the sample that changes the spectral profile of the light returning from the sample. In this case, subtraction of $I_S(\omega)$ and $I_R(\omega)$ before the Fourier transform is feasible. However, this is not necessary. If the individual spectra are left in the spectral interferogram, they will appear as a background feature centered around zero in the time domain.

The previous example is for a simple case in which light is returned from only one depth in the sample. More complex sample structures, such as biological tissues, will lead to multicomponent spectral interferograms. However, the mathematical treatment remains simple, requiring only Fourier transformation of the spectral interferogram to obtain signal intensity as a function of depth.

3. Interferometer Design and Characterization

Because SI uses a fixed interferometer, it is possible for the sample and reference arms to share the same beam path, as shown in Fig. 2. Instead of using a separate reference arm, the reference plane is defined by an optical surface near the front surface of the sample. In this case we use a 3-mm-thick glass flat. A sample is attached directly to the back of the glass plate. The back surface of the glass plate (the surface in contact with the sample) serves as a reference mirror. The front surface of the glass plate is far enough in front of the reference plane that it does not contribute to the spectral interferogram. This arrangement provides a well-determined positioning of the front surface of the sample, automatic compensation for dispersion or polarization differences in the sample and reference arms up to the point of the sample, and perfect overlap of the reflected sample and reference beams. Also, if a sample is to be kept in water, the cell containing the sample can be sealed directly to the glass plate with an O ring.

As discussed by Rollins and Izatt, an optimal reference arm power reflectivity[9] can be used to approach the shot-noise limit in OCT measurements. In a typical two-arm interferometer, the reference power is attenuated by insertion of neutral-density filters in the beam path or by adjustment of the reflectivity of the reference optic. In the common-path interferometer, it is not possible to attenuate the reference arm independently of the sample arm by use of filters. However, the reflectivity of the flat optic used to create the reference plane can be optimized by use of antireflection or partially reflecting coatings. When a glass flat is used for the reference plane and the sample is mounted in water directly in contact with the glass surface, the reference reflectivity is 3.6×10^{-3}, calculated by use of indices of refraction of 1.5 for glass and 1.33 for water. According to Rollins and Izatt, the optimal reflectivity is approximately 1.5×10^{-3}. Thus the reference reflectivity for samples immersed in water is close to optimal when the common-path interferometer is used.

The SI was constructed with a 50/50 cube beam splitter, an axial gradient-index lens ($f = 2.52$ cm), and a glass slide. The beam splitter is simply used to direct the interferometer signal to the spectrograph. The spectrograph consists of a $\frac{1}{4}$-m imaging spectrometer (Chromex Corp.) and a cooled 16-bit, 256×532 pixel CCD camera (C7041, Hamamatsu). The light source is a 850-nm AlGaAs superluminescent diode (SLD) with a 15-nm full-width-at-half-maximum spectral bandwidth (LDN-16, Volga Technology). The sample is mounted on a three-axis motorized translation stage. The CCD camera and translation stage are computer controlled.

In low-coherence interferometry the light-source

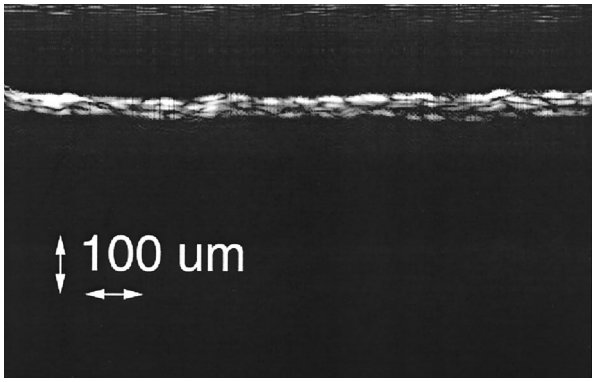

Fig. 3. Cross-sectional SI image of the outer skin of an onion. The cell structure is visible.

bandwidth determines the theoretical limit for the axial resolution. However, in SI, the design of the spectrograph affects the axial resolution and the depth range. Greater spectral dispersion increases the depth range. However, overfilling the camera and clipping the wings of the spectral interferogram will decrease the axial resolution. The dispersion of the $\frac{1}{4}$-m spectrograph is reasonably well matched to the SLD light-source bandwidth. Using samples constructed of thin glass plates and spacers of known thickness, we measured an axial resolution of 28 ± 3 μm. (This resolution is limited by the spectrograph. The SLD bandwidth's limited axial resolution is 23 ± 2 μm. Improved resolution can be easily achieved by use of a greater bandwidth SLD and appropriate spectrograph.) The free-space depth range is 2.8 mm. The lateral resolution is 10 ± 2 μm, measured with a Ronchi grating.

To successfully obtain images in scattering media with SI, it is necessary to measure small interference signals on top of a large dc background [see Eq. (1)]. Thus we chose a 16-bit CCD camera that is expected to provide a maximum dynamic range of 96 dB. Using the method of Häusler and Lindner,[5] we measured the dynamic range of the instrument as 76 dB. The dynamic range is not noise limited. It is limited by the dc background inherent to SI, which cannot be removed by simple averaging.

We compared the vibrational sensitivity of the common-path interferometer to a dual-arm configuration by introducing a vibration to the sample in each case. The common-path interferometer is easily converted into a dual-arm interferometer by the addition of a mirror and an attenuating neutral-density filter at the open position of the beam splitter (i.e., at the top of the beam splitter in Fig. 2). A pager buzzer was put in contact with a sample constructed of glass slides and spacers that provides strong interference signals. The vibrational amplitude was increased until the signal from the dual-arm interferometer was no longer detectable. The second (reference) arm was then blocked, and the same vibration was applied to the sample of the common-path interferometer. At a buzzer voltage at which the signal becomes undetectable in the dual-arm configuration, the signal decreases by only 20% for the single-arm configuration. This demonstrates

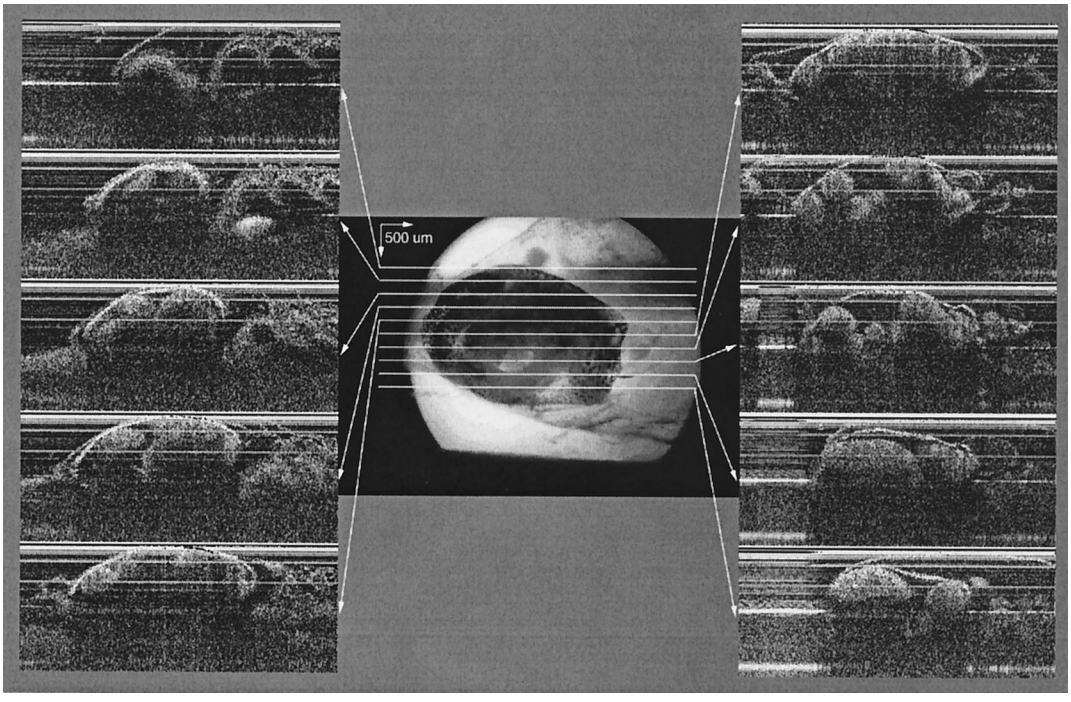

Fig. 4. Center: optical microscope image of the abdominal region of a *Xenopus laevis* tadpole viewed from the ventral surface. The head is to the right. Left and right: sagittal cross-sectional SI images. White lines drawn on the microscope image show the locations of the SI scans. The image-intensity gray scale is logarithmic. The lower three SI images on the right of the figure show streaked regions on their left sides where the scans exit the tadpole body. The center photograph and SI images are drawn to the same scale.

that the common-path interferometer is more stable and less sensitive to vibrations than a conventional dual-arm Michelson interferometer.

4. Imaging of Biological Samples

To demonstrate the capabilities of this SI for biological applications, we obtained cross-sectional images of onion skin and *Xenopus laevis* (African clawed frog) tadpole internal organs. Figure 3 shows an image of the outer skin of an onion. The sample was attached to the glass plate through a spacer to provide spatial separation from the reference plane. The thickness of the onion skin measured by a caliper is approximately 50 μm, which is in good agreement with the image shown in Fig. 3. The cell structure is clearly visible.

Xenopus laevis tadpoles have been frequently used by the research community as an animal model for evaluating *in vivo* optical imaging with OCT. For this reason, we also chose to image *Xenopus* tadpoles by using SI. Killed tadpoles, purchased as a mix of stages 40–47 from NASCO, were used.[10]

Figure 4 shows sagittal cross-sectional SI images of the abdominal region of a *Xenopus* tadpole. The photograph in the center of Fig. 4 was taken through an optical microscope from the ventral surface. In this figure, the head of the animal is to the right, outside the field of view. The abdominal area of the tadpole is clearly visible in the photograph, especially the intestines and stomach. The white lines on the photograph indicate where SI lateral scans were taken. We made the registration between the microscope image and the SI scans by marking the sample under the microscope, aligning the laser beam and lateral scan axis to these marks, and using the coordinates of the computer-controlled sample stage to determine the scan position and length.

The SI images are sagittal cross-sectional images in which the horizontal axis is the direction of the lateral scans and the vertical axis is depth. Zero depth, indicating the ventral surface, is at the top of the image. The scans go into the depth of the tadpole from the ventral surface shown in the photograph. The image-intensity gray scale is logarithmic. Structures corresponding to the internal organs, including intestines, stomach, diaphragm, and heart are visible in the SI images. The quality of these images compare favorably with early published OCT images obtained with a similar dynamic range.[11,12]

5. Summary

Spectral interferometry is a low-coherence interferometric technique that holds promise for video-rate biological imaging with simpler instrumentation than time-domain OCT. Frequency-domain OCT can be implemented with a simple, stable spectral interferometer design in which the reference and sample arms share the same path. The advantages of the common-path interferometer include greater ease of alignment, reduced sensitivity to vibration and greater stability due to automatically maintained beam overlap, and nearly optimal reference arm reflectivity when the interferometer is used to image samples immersed in water. This interferometer configuration can be easily implemented with fiber optics.

The SI images presented here were obtained with the CCD frame rate at its maximum, without averaging of frames or postacquisition image processing. The imaging rate is limited by the CCD camera's data readout rate (140 Hz with the present CCD camera). Thus two-dimensional images consisting of 100 axial scans can be obtained at a rate of 1.4 Hz. Faster cameras are available that will allow useful real-time imaging rates of 10 Hz or more, depending on image size. Using the two-dimensional capabilities of the CCD camera will allow fast acquisition of three-dimensional images because scanning of the light beam is required in only one dimension when line illumination is used. Further research is in progress to increase the dynamic range of frequency-domain OCT by use of a differential technique that removes the spectral background, autocorrelation signals, and other dc artifacts from SI images. Recent results show that a dynamic range of 100 dB or more is feasible.[13]

This study was supported by The National Heart, Lung, and Blood Institute of the National Institutes of Health under grant R43 HL69108-01.

References and Notes

1. W. Drexler, U. Morgner, F. X. Kärtner, C. Pitris, S. A. Boppart, X. D. Li, E. P. Ippen, and J. G. Fujimoto, "*In vivo* ultrahigh-resolution optical coherence tomography," Opt. Lett. **24,** 1221–1223 (1999).
2. G. J. Tearney, B. E. Bouma, and J. G. Fujimoto, "High-speed phase- and group-delay scanning with a grating-based phase control delay line," Opt. Lett. **22,** 1811–1813 (1997).
3. A. M. Rollins, M. D. Kulkarni, S. Yazdanfar, R. Ungarunyawee, and J. A. Izatt, "*In vivo* video rate optical coherence tomography," Opt. Express **3,** 219–229 (1998), http://www.opticsexpress.org.
4. A. F. Zuluaga and R. Richards-Kortum, "Spatially resolved spectral interferometry for determination of subsurface structure," Opt. Lett. **24,** 519–521 (1999).
5. G. Häusler and M. W. Lindner, "Coherence radar and spectral radar—new tools for dermatological diagnosis," J. Biomed. Opt. **3,** 21–31 (1998).
6. L. Lepetit, G. Chériaux, and M. Joffre, "Linear techniques of phase measurement by femtosecond spectral interferometry for applications in spectroscopy," J. Opt. Soc. Am. B **12,** 2467–2474 (1995).
7. M. W. Lindner, P. Andretzky, F. Kiesewetter, and G. Häusler, "Spectral radar: optical coherence tomography in the Fourier domain," in *Handbook of Optical Coherence Tomography*, B. E. Bouma and G. J. Tearney, eds. (Marcel Dekker, New York, 2002), pp. 335–357.
8. M. Wojtkowski, A. Kowalczyk, R. Leitgeb, and A. F. Fercher, "Full range complex spectral optical coherence tomography technique in eye imaging," Opt. Lett. **27,** 1415–1417 (2002).
9. A. M. Rollins and J. A. Izatt, "Optimal interferometer designs for optical coherence tomography," Opt. Lett. **24,** 1484–1486 (1999).
10. Killed tadpoles were used to comply with National Institutes of Health regulations regarding the use of live, vertebrate ani-

mals. (We do not have approval for experimentation that uses live vertebrates.) This SI method should be as applicable to live, *in vivo* measurements as time-domain OCT, although this remains to be demonstrated.
11. D. Huang, E. A. Swanson, C. P. Lin, J. S. Schuman, W. G. Stinson, W. Chang, M. R. Hee, T. Flotte, K. Gregory, C. A. Puliafito, and J. G. Fujimoto, "Optical coherence tomography," Science **254,** 1178–1181 (1991).
12. G. J. Tearney, B. E. Bouma, S. A. Boppart, B. Golubovic, E. A. Swanson, and J. G. Fujimoto, "Rapid acquisition of *in vivo* biological images by use of optical coherence tomography," Opt. Lett. **21,** 1408–1410 (1996).
13. A. B. Vakhtin, K. A. Peterson, W. R. Wood, and D. J. Kane, "Differential spectral interferometry: an imaging technique for biomedical applications," Opt. Lett. **28,** 1332–1334 (2003).